Geophysical Research Letters

Supporting Information for

Sub-seasonal changes observed in subglacial channel pressure, size, and sediment transport

Florent Gimbert[1,2]*, Victor C. Tsai[1,2], Jason M. Amundson[3], Timothy C. Bartholomaus[4], Jacob I. Walter[4]

[1] Seismological Laboratory, California Institute of Technology, Pasadena CA, USA
[2] Division of Geological and Planetary Sciences, California Institute of Technology, Pasadena CA, USA
[3] Department of Natural Sciences, University of Alaska Southeast, Juneau AK, USA
[4] Institute for Geophysics, University of Texas Austin, Austin TX, USA

Contents of this file

Introduction

The robustness of Mendenhall Glacier discharge data as inferred from mass conservation of the glacier terminating lake is demonstrated in Text S1. Error estimates on model predictions due to uncertainty in channel shape and apparent flow roughness are provided in Text S2 and S3, respectively. Likelihood of unfilled subglacial conduits nearby the AMBR seismic station is discussed in Text S4. Finally, estimates of absolute pressure and effective stress are made in Text S5, in which we also discuss how our seismological framework could be used to constrain basal friction laws in future work.

Text S1. Analysis of discharge data

Our Mendenhall Glacier discharge dataset (see Fig. 2B) is inferred from mass conservation of the glacier terminating lake. Since all streams feeding the lake were not gauged during the time period of the seismic experiments, these indirect measurements rely on the assumption that lake inflow from the other stream sources is small or co-varies with that of the Mendenhall Glacier. Here we test this assumption in two ways. First, we compare our inferred discharge with those from the main contributing stream Nugget Creek, which was gauged from year

2000 to year 2004 (see Fig S1). We find that Nugget Creek only accounts for about 10 to 30% of total discharge, and systematically co-varies with total discharge. Second, we verify that this picture is not modified when adding the contribution of all other potential streams feeding the lake. To do so, we predict total discharge from melt and rain for all basins draining into the lake and compare with predicted discharge from the Mendenhall Glacier catchment only. Our predictions use a SRTM DEM to create an area-altitude distribution for each draining catchment, and discharge from melt and rain is calculated using temperature and precipitation records from the Juneau airport. We find the area for which T>0 °C using an adiabatic lapse rate of 0.0071 °C m^{-1}, and we multiply that area by the precipitation rate to obtain discharge from rain and by a degree day factor of $6 \cdot 10^{-3}$ m d^{-1} °C^{-1} to obtain discharge from melt. Rain discharge calculations include valley walls, and melt discharge calculations are only performed on glaciated areas (snow is neglected). Storage and evapotranspiration are neglected. These calculations confirm that the Mendenhall Glacier is the main source of discharge into the Mendenhall Lake, since time-series of total discharge almost superimpose with time-series of discharge from the Mendenhall Glacier (Fig. S2). We thus conclude that our indirect measurements of discharge into the lake properly approximate discharge from the Mendenhall Glacier.

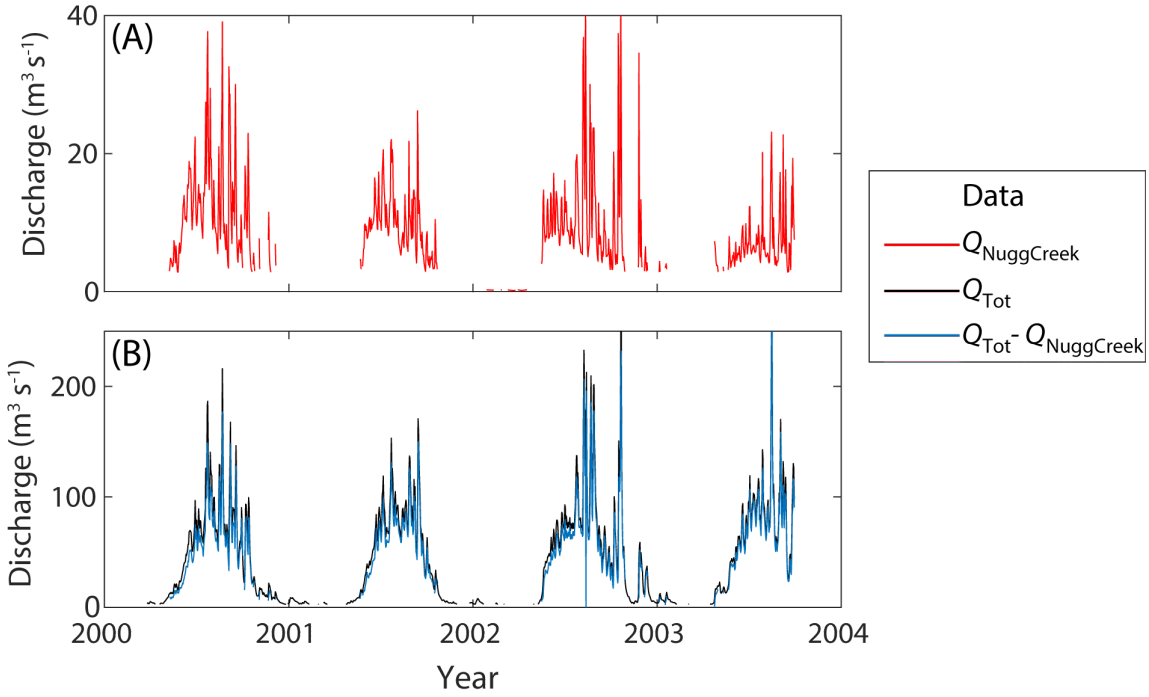

Fig. S1: Comparison of Nugget Creek discharge $Q_{NuggCreek}$ into Mendenhall Lake as measured by a stream gauge over the period 2000-2004 (A, red line) with total discharge Q_{Tot} as measured from mass conservation (B, black line). Nugget Creek is the second largest lake water input contributor after Mendenhall Glacier, but only represents about 10 to 30% of total discharge, the rest being almost entirely due to Mendenhall Glacier (B, blue line, see also Fig. S2).

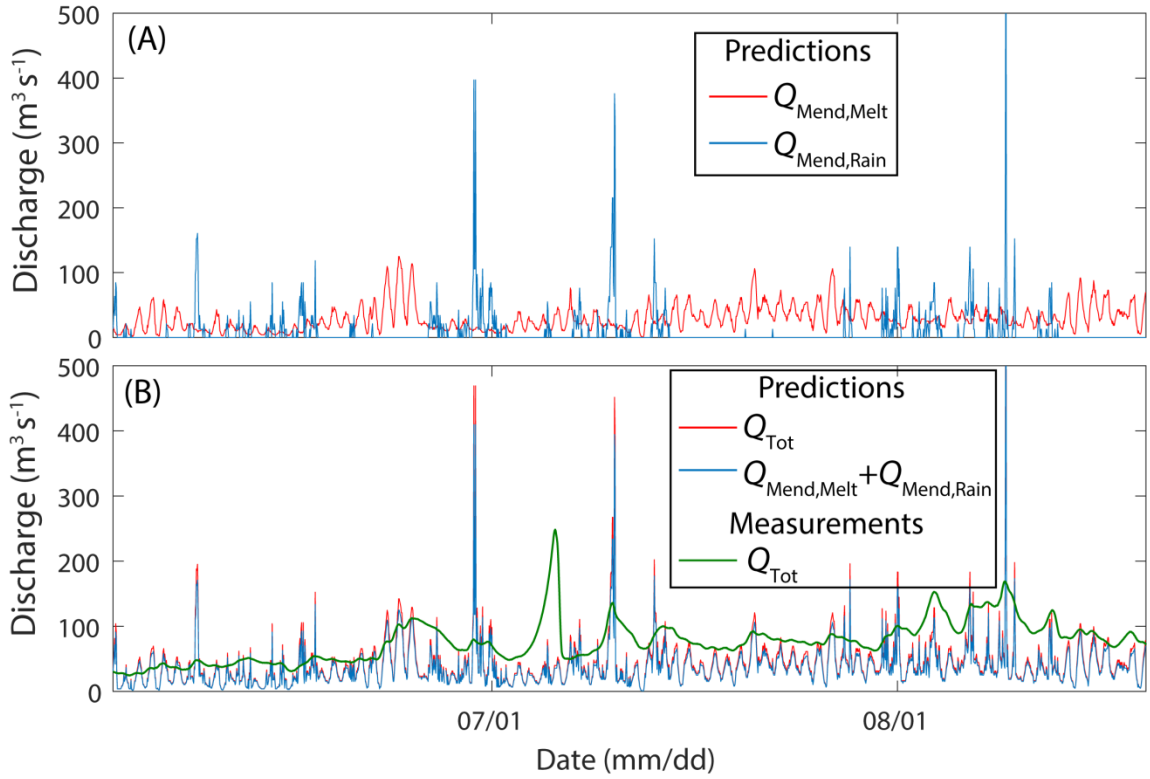

Fig. S2: Predicted and observed discharge in the Mendenhall Glacier terminating lake. (A) Discharge from melt (in red) and rain (in blue) as predicted in the Mendenhall Glacier catchment from air temperature and precipitation data recorded at the Juneau airport. (B) Total discharge (melt plus rain) as observed (green line) and predicted (red and blue lines) in the lake terminating glacier. The red line shows predictions for all catchments draining into the lake, and the blue line shows predictions restricted to the Mendenhall Glacier catchment. Note that transient water storage into the glacier causes the glacier output discharge (green line) to be much smoother than the predicted glacier input discharge (blue line). Also noticeable is the large deviation between modeled and observed discharge observed on July 3-7, which is caused by the Suicide Basin lake drainage event (see main text).

Text S2. Control of channel shape on model predictions

Here we evaluate the control of channel shape on the predicted scalings of seismic power P_w, channel hydraulic pressure gradient S and channel hydraulic radius R as obtained in equations 4 and 5 of the main text. Various channel shapes are explored by defining the conduit angle θ_c, the channel water angle θ_w and the conduit radius r_c as shown in Fig. S3A. For such channel shape, the wetted perimeter Γ is defined as

$$\Gamma(r_c,\theta_c,\theta_w)=2r_c(\theta_w+\sin\theta_c) \quad \text{(S1)}$$

and the area flow A is defined as

$$A(r_c,\theta_c,\theta_w) = \begin{cases} r_c^2\left[\theta_w \sin^2\theta_c + \sin(\theta_c-\theta_w)[\cos(\theta_c-\theta_w) - \cos\theta_c]\right], \theta_c \le \pi/2 \\ r_c^2\left[\theta_w - \frac{1}{2}\sin 2\theta_c - \frac{1}{2}\sin\left(2(\theta_c+\theta_w)\right)\right], \ \theta_c \ge \pi/2. \end{cases} \quad \text{(S2)}$$

Thus we have $A=\Gamma^2/\beta$, $\Gamma=\beta R$ and $A=\beta R^2$ as defined in the main text, with β given by

$$\beta(\theta_c,\theta_w) = \begin{cases} \dfrac{4(\theta_w+\sin\theta_c)^2}{\theta_w \sin^2\theta_c + \sin(\theta_c-\theta_w)[\cos(\theta_c-\theta_w) - \cos\theta_c]}, & \theta_c \le \dfrac{\pi}{2} \\ \dfrac{4(\theta_w+\sin\theta_c)^2}{\left[\theta_w - \frac{1}{2}\sin 2\theta_c - \frac{1}{2}\sin\left(2(\theta_c+\theta_w)\right)\right]}, & \theta_c \ge \dfrac{\pi}{2}, \end{cases} \quad \text{(S3)}$$

along with the particular solutions $\beta_{sc}=4(1+\theta_w)^2/\left(\theta_w+\frac{1}{2}\sin 2\theta_w\right)$ for a perfectly semi-circular conduit ($\theta_c = \pi/2$), and $\beta_c=4\theta_w^2/\left(\theta_w-\frac{1}{2}\sin 2\theta_w\right)$ for a perfectly circular conduit ($\theta_c = \pi$).

To evaluate uncertainties on the predicted scalings, we consider reasonable values of θ_c and θ_w. We vary θ_c from π/6 to π and θ_w from π/6 to π/2 if $\theta_c<\pi/2$ or from π/6 to θ_c if $\theta_c \ge \pi/2$, and evaluate the error due to variations in β as

$$E(X,\theta_c) = \frac{1}{2}\frac{\max(\beta(\theta_w)^X) - \min(\beta(\theta_w)^X)}{<\beta(\theta_w)^X>}, \quad \text{(S4)}$$

where <> indicates averaging and X is an exponent. Error on the scaling of P_w for constant pressure gradient (see equation 4.2. of the main text) is calculated using X=1/4, and is shown on Fig. S3B. Error on predicted P_w is of about 10% for semi-circular, elongated conduits ($\theta_c<\pi/2$) and of about 25% for more circular conduits ($\theta_c>\pi/2$). These variations are thus of at least an order of magnitude smaller than those of $Q^{5/4}$, which typically varies by about a factor of 2 to a factor of 5 at the various timescales of interest (see Fig. 2 and Fig. 3). $P_w \propto Q^{5/4}$ is thus a good approximation of seismic power changes with discharge for channels evolving at constant pressure gradient, regardless of conduit shape and degree of fullness. We note, however, that uncertainties on conduit shape and fullness precludes us from confidently interpreting seismic power changes smaller than $10\log_{10}(1.25)$=1 dB. The associated uncertainty in our inferred values of R and S can be estimated from a similar analysis on the scalings of R and S expressed with β as

$$\begin{aligned} S &\sim \beta^{6/41} P_w^{24/41} Q^{-30/41} \\ R &\sim \beta^{33/82} P_w^{-9/82} Q^{21/41}. \end{aligned} \quad \text{(S5)}$$

We calculate uncertainty using X=6/41 for S and X=33/82 for R in equation (S4). We find that uncertainty on channel shape causes about 4% to 8% uncertainty in our inferred values of hydraulic pressure gradient S depending on whether conduits are more semi-circular or

circular, respectively (Fig. S3C). Uncertainties in the inferred channel hydraulic radius R are larger, and correspond to 10% to 20% for semi-circular and circular conduits, respectively. Thus, variations of S that are smaller than 8% change or of R that are smaller than 20% change cannot be interpreted with confidence. Such uncertainties are shown as the light blue region for R on Fig. 2B, but are not shown for S since uncertainty on pressure gradient is dominated by apparent flow roughness uncertainty rather than by uncertainty on conduit shape (see the next section).

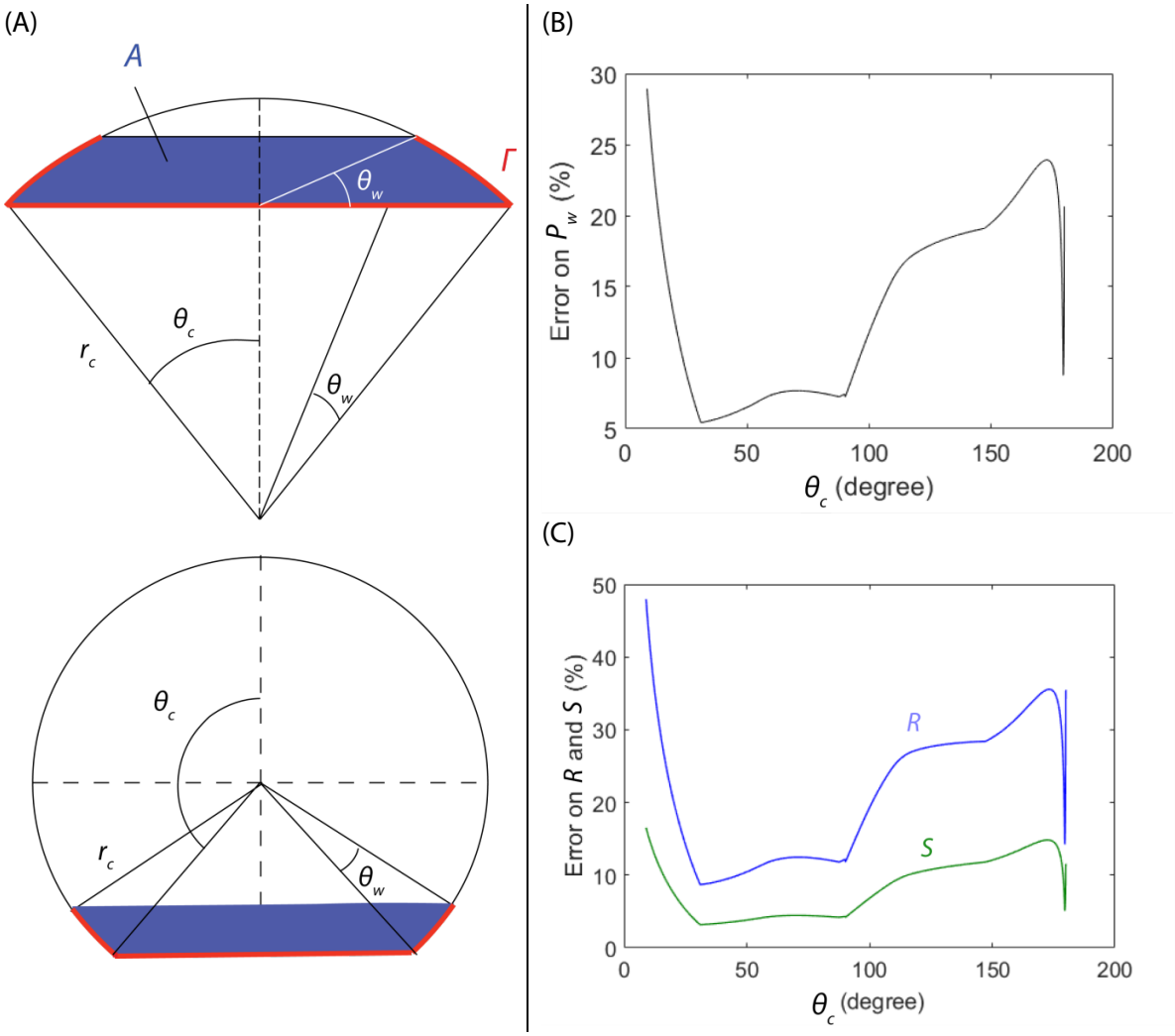

Fig. S3: Error estimates on the scalings of P_w, S and R due to uncertainty in channel shape. (A) Sketches of the various possible conduit and channel shapes evaluated for uncertainty, and definition of the conduit angle θ_c, the channel water angle θ_w and the conduit radius r_c. (B) Percent error on P_w from unfilled to filled conduits as a function of conduit angle θ_c. (C) Percent error on R (blue) and S (green) from unfilled to filled conduits as a function of conduit angle θ_c.

Text S3. Control of flow apparent roughness on model predictions

Here we evaluate uncertainties on hydraulic radius R and hydraulic pressure gradient S due to neglecting changes in apparent flow roughness H/k_s in the main text, i.e. due to neglecting function ζ in model predictions (see equation 1 of main text). Keeping function ζ in model derivations, the pressure gradient S_ζ and hydraulic radius R_ζ can be expressed as

$$R_\zeta \sim \zeta\left(\frac{H}{k_s}\right)^{\frac{9}{82}} R_{\text{ref}}\left(\frac{P_w}{P_{w,\text{ref}}}\right)^{\frac{9}{82}}\left(\frac{Q}{Q_{\text{ref}}}\right)^{\frac{21}{41}} \sim \zeta\left(\frac{H}{k_s}\right)^{\frac{9}{82}} R$$
$$S_\zeta \sim \zeta\left(\frac{H}{k_s}\right)^{-24/41} S_{\text{ref}}\left(\frac{P_w}{P_{w,\text{ref}}}\right)^{24/41}\left(\frac{Q}{Q_{\text{ref}}}\right)^{-30/41} \sim \zeta\left(\frac{H}{k_s}\right)^{-24/41} S \quad \text{(S6)}$$

R_ζ thus depends weakly on $\zeta(H/k_s)$ such that uncertainties in R due to neglecting $\zeta(H/k_s)$ are small (5-10%, see Fig. S4), but S_ζ depends more strongly on $\zeta(H/k_s)$ and error can be up to 30-50% (see Fig. S4) if H/k_s varies by up to a factor of 10. This error range for S is shown as the light green region on Fig. 2B, but is not shown for R since error on channel shape dominates for this parameter (see previous section). Such relatively large uncertainties on S could explain its apparent variations when conduits are interpreted to be unfilled (see Fig. 2B). With the present state of knowledge, however, accounting for changes in $\zeta(H/k_s)$ in model predictions is not feasible, since this would require inverting for absolute flow depth in channels from the seismic signal, i.e. modeling the absolute amplitude of the recorded noise.

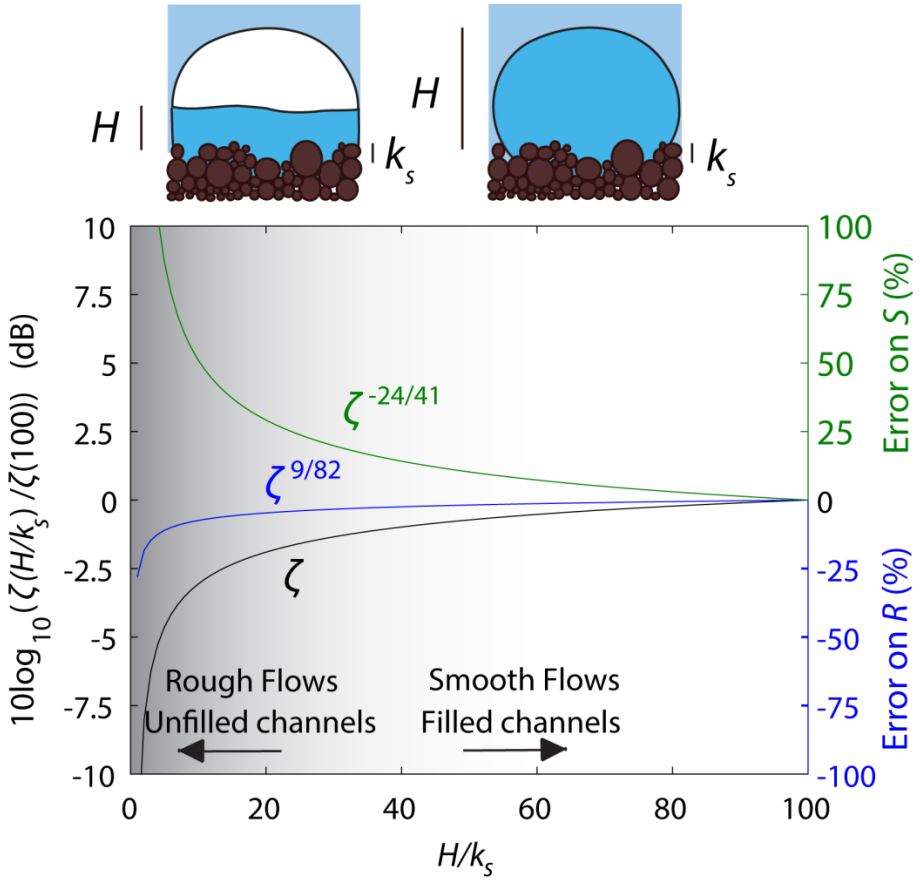

Fig. S4: Function ζ (in black) as calculated from equation 33 of *Gimbert et al.* (2014) as a function of H/k_s, and errors caused by neglecting ζ in the model inversions of R (blue) and S (green).

Text S4. Likelihood of partially filled subglacial conduits nearby the AMBR seismic station

Here we test the likelihood of partially filled subglacial conduits nearby the AMBR seismic station, as interpreted in the main text. We solve for conduit closure rate as $\frac{dA(t)}{dt} = -c\,\sigma_i^n A(t)$ (solution: $A(t) = A_0 \exp(-c\,\sigma_i^n t)$) where A is conduit area, A_0 is a constant, $c = 1 \cdot 10^{-24}$ Pa^{-3} s^{-1} and $n=3$ are constants related to ice viscosity for temperate glaciers [*Cuffey and Paterson*, 2010; *Schoof*, 2010] and $\sigma_i = \rho_i g h_i$ is effective pressure (for channels at atmospheric pressure), ρ_i=900 kg m^{-3} being ice density and g=9.81 m s^{-2} being acceleration due to gravity. Glacier thickness h_i near the seismic and GPS stations is not well known (radar measurements have only been conducted relatively far (~1 km) upstream or downstream, see *Motyka et al.* [2003]), but 100-300 m can be inferred as reasonable upper and lower estimates on thickness. Though conduit closure occurs relatively rapidly (within a couple of days) for 300 m thick ice, its strong dependence on ice thickness causes closure timescales to be much longer (at least a week) for ice thinner than 200 m (Fig. S5). Given uncertainties on ice thickness, we conclude that conduits can plausibly remain unfilled over days- to week-long time preiods.

We also note that, in the context of lake terminating glaciers like the Mendenhall Glacier, subglacial conduits could be filled by the lake if located at lower elevation than the lake surface elevation. Nearby station AMBR, however, glacier bed elevation is likely higher than the lake surface elevation, since glacier surface elevation at that location is higher than 300 m while glacier thickness is expected to be at most 300 m. Subglacial conduits causing ground motion at AMBR are thus unlikely to be filled by water flowing from the lake.

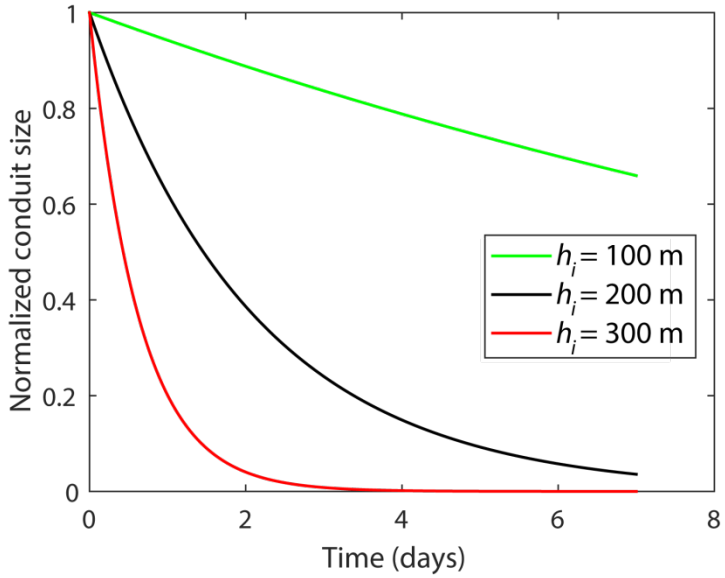

Fig. S5: Estimated conduit size decrease by ice creep as a function of time for various glacier thicknesses.

Text S5. Estimate of absolute water pressure and correlation between water pressure gradient and glacier surface speed

Basal hydraulic pressure gradient S inferred from seismic noise analysis (see Fig. 2B) during the early melt season (June 3-26) is shown as a function of glacier sliding velocity measured from the GPS station IPA5 on Fig. S6. Though the data are relatively scattered, we find a significant positive correlation coefficient of 0.61 between these two quantities. To test whether this positive correlation is supported by absolute water pressure p being a significant fraction of overburden pressure σ_i, we convert the relative hydraulic pressure gradient S to an absolute hydraulic pressure gradient S_a using unfilled conduits as a reference, in which case $S_{a,\text{unfilled}}$ for unfilled conduits simply corresponds to basal glacier slope $\tan\theta$. We roughly approximate $S_{a,\text{unfilled}}=\tan\theta$ as 0.1±0.05 from surface glacier elevation measurements [*Motyka et al.*, 2003] and we estimate the absolute pressure gradient S_a at any time t as

$$S_a(t)=\frac{1}{0.8}\frac{S(t)}{S^{\text{ref}}}S_{a,\text{unfilled}}, \tag{S7}$$

where the normalization coefficient of 0.8 comes from the approximation of $\frac{S_{\text{unfilled}}}{S^{\text{ref}}}$ for unfilled conduits (Fig. 2B). Assuming that pressure gradient measured from noise nearby the seismic station is constant over the distance $d\approx1\pm0.1$ km between the seismic station and the glacier terminus, we estimate the absolute subglacial water pressure at the level of the seismic station as (using equation S7)

$$S_a(t)=\rho g d\left(S_a(t)-S_{a,\text{unfilled}}\right)=\rho g d S_{a,\text{unfilled}}\left(\frac{1}{0.8}\frac{S(t)}{S^{\text{ref}}}-1\right). \tag{S8}$$

We obtain $p_{\max}=2.4\pm1.2$ MPa (using $\rho=1000$ kg m^{-3} and $g=9.81$ m s^{-2}) when maximum sliding occurs during flood 1, i.e. when $\frac{S}{S^{\text{ref}}}\approx2.5$ (flood 1, June 21-26 in Fig. 2B). To compare $p_{\max}$ with overburden pressure σ_i, we calculate σ_i as

$$\sigma_i=\rho_i g h_i\approx1.76\pm0.85 \text{ MPa} \tag{S9}$$

where $\rho_i=900$ kg m^{-3} is ice density and $h_i\approx100$-300 m is glacier thickness. $p_{\max}$ is thus of the order of and potentially larger than σ_i, and thus basal effective stresses at the location of channels is likely strongly modified by water pressure over the melt season, consistent with fluctuations of S being correlated with glacier sliding velocity (Fig. S6). Properly comparing the observed relationship between sliding velocity and subglacial water pressure with that predicted by existing sliding laws, however, requires reliable information on the area covered by channels and the nearby hydrological network, i.e. on the area over which the measured pressure is applied, which is unknown. Future seismic array processing and/or numerical modeling work with appropriate knowledge of bed topography could help determine this, and thus allow for the use of these observational constraints to test and improve sliding laws.

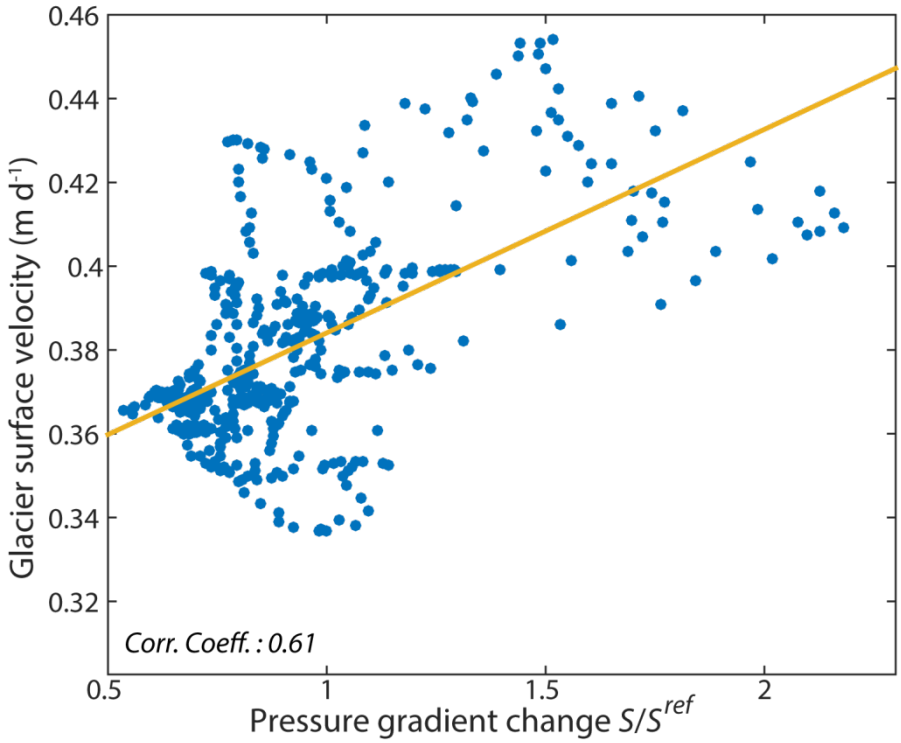

Fig. S6: Observed glacier surface velocity as a function of observed subglacial channel pressure gradient. Data have been selected during the early melt season (June 3-26). The continuous line shows best linear fit.

REFERENCES

Cuffey, K. M., and W. S. B. Paterson (2010), *The Physics of Glaciers, Fourth Edition*, 4 edition., Academic Press, Burlington, MA.

Motyka, R. J., S. O'Neel, C. L. Connor, and K. A. Echelmeyer (2003), Twentieth century thinning of Mendenhall Glacier, Alaska, and its relationship to climate, lake calving, and glacier run-off, *Glob. Planet. Change*, *35*(1–2), 93–112, doi:10.1016/S0921-8181(02)00138-8.

Schoof, C. (2010), Ice-sheet acceleration driven by melt supply variability, *Nature*, *468*(7325), 803–806, doi:10.1038/nature09618.